# Dynamic Inhomogeneity in the Photodynamics of Cyanobacterial Phytochrome Cph1

Peter W. Kim,[†] Nathan C. Rockwell,[‡] Shelley S. Martin,[‡] J. Clark Lagarias,[‡] and Delmar S. Larsen*,[†]

[†]Department of Chemistry and [‡]Department of Molecular Cellular Biology, University of California at Davis, One Shields Avenue, Davis, California 95616, United States

S *Supporting Information*

ABSTRACT: Phytochromes are widespread red/far-red photosensory proteins well known as critical regulators of photomorphogenesis in plants. It is often assumed that natural selection would have optimized the light sensing efficiency of phytochromes to minimize nonproductive photochemical deexcitation pathways. Surprisingly, the quantum efficiency for the forward P_r-to-P_{fr} photoconversion of phytochromes seldom exceeds 15%, a value very much lower than that of animal rhodopsins. Exploiting ultrafast excitation wavelength- and temperature-dependent transient absorption spectroscopy, we resolve multiple pathways within the ultrafast photodynamics of the N-terminal PAS-GAF-PHY photosensory core module of cyanobacterial phytochrome Cph1 (termed Cph1Δ) that are primarily responsible for the overall low quantum efficiency. This inhomogeneity primarily reflects a long-lived fluorescent subpopulation that exists in equilibrium with a spectrally distinct, photoactive subpopulation. The fluorescent subpopulation is favored at elevated temperatures, resulting in anomalous excited-state dynamics (slower kinetics at higher temperatures). The spectral and kinetic behavior of the fluorescent subpopulation strongly resembles that of the photochemically compromised and highly fluorescent $Y_{176}H$ variant of Cph1Δ. We present an integrated, heterogeneous model for Cph1Δ that is based on the observed transient and static spectroscopic signals. Understanding the molecular basis for this dynamic inhomogeneity holds potential for rational design of efficient phytochrome-based fluorescent and photoswitchable probes.
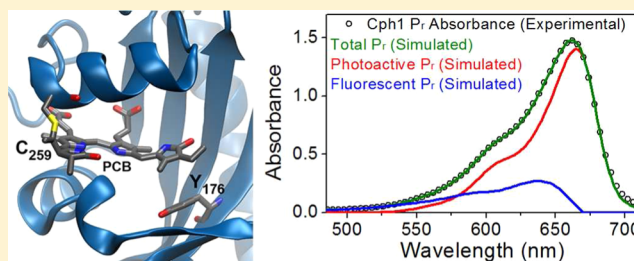
Phytochromes are photoreceptors first discovered in plants, where they function as critical developmental regulators, and later found in fungi, bacteria, and algae.[1,2] Phytochromes utilize photoisomerization of a covalently attached, heme-derived linear tetrapyrrole (bilin) chromophore (Figure 1) to photoconvert between two states. Phytochromobilin and phycocyanobilin chromophores are incorporated in plant and cyanobacterial phytochromes, respectively. Both proteins possess red/far-red photocycles in which their dark-stable, red-absorbing P_r state (peak absorption at 640−680 nm) reversibly photointerconverts with a metastable far-red-absorbing P_{fr} photoproduct (700−740 nm). Photoconversion effects structural changes that are subsequently transduced by cellular signaling pathways. In plants, phytochromes regulate many processes, including germination, shade avoidance, and flowering.[3] Phytochrome engineering in crop plants thus holds great agronomic potential.

Red/far-red photocycles of phytochromes are well separated from those of blue-sensing photoproteins, leading to increasing focus on phytochromes as reporters for biological imaging and as a basis for red-responsive modules in synthetic biology.[4−6] In such applications, high quantum yields are desirable. The excited-state population generated upon photoexcitation undergoes productive photoisomerization and fluorescence, with quantum yields denoted by Φ_{photo} and Φ_{fluor}, in addition to other nonradiative deexcitation pathways. Despite the avail-

ability of crystal structures and multiple spectroscopic studies, our understanding of the photodynamic processes immediately following photoexcitation does not adequately explain the observed fluorescence and photochemical quantum efficiencies of plant and cyanobacterial phytochromes. Photoisomerization of the bilin 15,16-double bond occurs with a low P_r-to-P_{fr} Φ_{photo} of <20% for nearly all known phytochromes, while the room-temperature P_r fluorescence yield can vary in a range of 0.1−3%.[6−8] Moreover, Φ_{photo} for phytochrome is lower than those reported for distantly related cyanobacteriochromes that use the same chromophore.[9−11] These data indicate that both Φ_{photo} and Φ_{fluor} reflect specific protein−chromophore interactions rather than an intrinsic property of bilins per se. Indeed, in different protein contexts (e.g., the phycobiliproteins and mutant apophytochromes), Φ_{fluor} for PCB chromophores can reach 100% at the expense of photochemistry.[12,13]

Excited-state decay of phytochromes is multiphasic, which has been interpreted in varying ways, including excited-state equilibrium,[14] partial Z-to-E isomerization in the excited state,[15] and excited-state proton transfer.[16] Despite support for a homogeneous P_r ground state,[17] ongoing studies of the
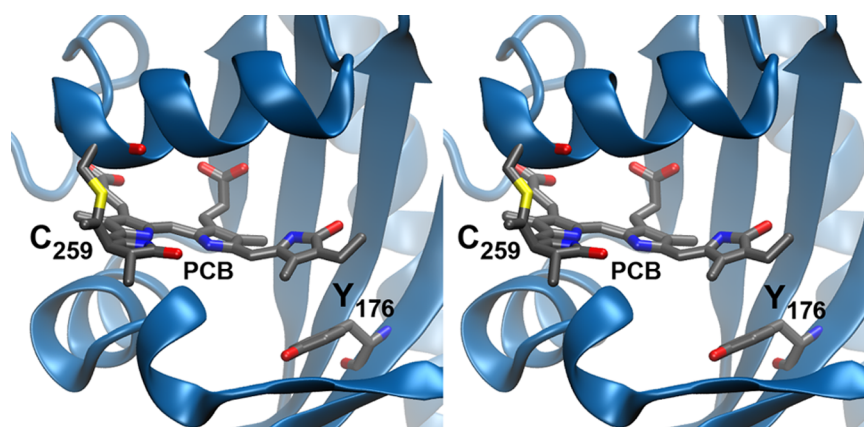
Figure 1. Stereodiagram showing protein−chromophore interactions in the Cph1Δ P$_r$ state.[20] The PCB chromophore is shown with Tyr176 and Cys259, which is covalently attached to PCB.

cyanobacterial phytochrome Cph1 from *Synechocystis* sp. PCC6803 implicate its heterogeneity,[18,19] providing the rationale for the investigation presented here. Cph1 from *Synechocystis* has proven to be an excellent model system for plant phytochromes because of its robust recombinant expression and the availability of a crystal structure for the conserved photosensory core module (Figure 1).[20,21] The full length Cph1 protein consists of a PAS-GAF-PHY photosensory core module (termed Cph1Δ) coupled to a C-terminal histidine kinase domain.

In Cph1, red light initiates the forward P$_r$-to-P$_{fr}$ conversion, affording the primary isomerized intermediate (Lumi-R) on a picosecond time scale.[15,22−26] Lumi-R subsequently evolves on the ground-state electronic surface via several spectroscopically distinct intermediates ultimately generating the P$_{fr}$ signaling state on an approximately millisecond time scale.[27,28] Primary Lumi-R formation for Cph1Δ has been studied with both electronic[22,23] and vibrational[15,24−26] transient spectroscopies, often with contradictory conclusions. All studies resolve multiexponential excited-state decay kinetics, typically ascribed to either complex nonexponential dynamics arising from a single ground-state population (the "homogeneous perspective") or an ensemble of ground-state subpopulations, each exhibiting single-exponential dynamics (the "inhomogeneous perspective"). Resonant Raman intensity analysis and hybrid quantum mechanics/molecular mechanics simulations support a homogeneous P$_r$ state,[29] also corroborated by earlier pump−dump−probe (PDP) studies.[23,24] In contrast, solid-state nuclear magnetic resonance (NMR) resolved two P$_r$ subpopulations: one structure consistent with the known crystal structure and a second interpreted as having a modified charge distribution and hydrogen bond network.[30] More recent PDP experiments also implicate a heterogeneous P$_r$ ground state for a red-absorbing cyanobacteriochrome (CBCR).[31] The fluorescence excitation spectrum of the Cph1Δ P$_r$ state exhibits a small but significant blue shift relative to the absorption spectrum.[18] Given that both are static measurements, this discrepancy is consistent with a blue-shifted fluorescent subpopulation (although it does not exclude distinct excited-state populations reflecting isomers across a low-barrier hydrogen bond). Moreover, equilibrium between such subpopulations could explain reversible temperature effects on the P$_r$ absorption band that have been attributed to thermal spectral broadening of a homogeneous population.[17]

Resolution of the question of P$_r$ ground-state heterogeneity has broad implications. If understood, ground-state heterogeneity of Cph1 not only will help reconcile conflicting interpretations of available spectroscopic and X-ray crystallographic data (discussed later) but also will inform our understanding of the merits and limitations of Cph1 as a model system for plant phytochromes. Additionally, a fluorescent subpopulation in wild-type Cph1 (WT) potentially provides a rationale for the behavior of the fluorescent, photochemically inactive Y$_{176}$H variant of Cph1 (YH), because this mutation in both Cph1 and plant phytochromes blue shifts the P$_r$ absorption maximum while also greatly increasing Φ$_{fluor}$. Here, we revisit the P$_r$ photodynamics for Cph1Δ using a combination of static fluorescence, temperature-dependent static/transient absorption, and excitation wavelength-dependent transient absorption spectroscopies for both WT and YH. Surprisingly, WT exhibits an inverted Arrhenius effect on excited-state decay, with faster decay occurring at lower temperatures. Using global analysis and singular-value decomposition (SVD), five coexisting ground-state subpopulations were resolved in thermal equilibrium, allowing quantitative interpretation of Φ$_{fluor}$ and Φ$_{photo}$ and reconciling various independent spectroscopic observations. Our study thus represents definitive evidence of Cph1 P$_r$ ground-state heterogeneity at ambient temperatures and also correlates the observed photodynamics of different coexisting excited-state subpopulations with observed rates and yields of double-bond photoisomerization.

■ EXPERIMENTAL PROCEDURES

Protein Purification. *Escherichia coli* strain LMG194 (Invitrogen) was cotransformed with two plasmids, pBAD-Cph1(N514)-CBD and pPL-PCB, to permit production of holo-Cph1Δ *in vivo*. Transformed cells were selected on rich medium (RM) plates containing 100 mg/mL ampicillin and 50 mg/mL kanamycin. An individual colony was cultured overnight in RM (AMP50 KAN25) and inoculated with a 1:500 ratio in 100 mL of RM. Upon reaching an optical density (OD) of 0.5 at 600 nm, the culture was transferred to 900 mL of LB (Luria-Bertani medium or lysogeny broth) containing 50 mg/mL ampicillin, 25 mg/mL kanamycin, and 1 mM isopropyl β-ᴅ-1-thiogalactopyranoside for a total expression of 6 L. After 1 h at 37 °C and after the sample had been shaken at 250 rpm in a shaker-incubator (Innova 4340 from New Brunswick Scientific), arabinose was added to a final concentration of

0.002% (w/v) followed by incubation for 1 h prior to a decrease in the temperature to 20 °C for 16 h. Subsequently, cells were harvested by centrifugation at 5000g for 10 min and stored at −80 °C. The pellet was resuspended at 1 g of wet weight/4 mL of lysis buffer A [25 mM Hepes-Na (pH 8.0), 500 mM NaCl, and 1 mM EDTA] and 0.1% (v/v) Triton X-100. Cells were lysed by two passes through a microfluidizer (M-110Y) at 15000 psi, and all subsequent steps were conducted at 4 °C. The crude lysate was clarified by centrifugation (35000 rpm, Ti-60 Beckman, 30 min) and applied to a 30 mL chitin column (New England Biolabs), which was washed thoroughly with buffer A at a rate of 1 mL/min. Intein-mediated cleavage was induced by flushing the column with 1 bed volume of elution buffer (buffer A and 1 mM dithiothreitol and overnight incubation at 4 °C). Eluted fractions containing Cph1Δ(N514) were pooled and concentrated in Amicon spin prep columns (10000 kDa cutoff) and dialyzed overnight at 4 °C in 1 L of buffer B [25 mM Tes-KOH (pH 8.0), 25 mM KCl, and 10% glycerol].

Transient Absorption Measurements. The primary light source was an amplified Ti:sapphire laser system (Spectra Physics Spitfire Pro) that delivered 1 kHz pulses at a λ_{center} of 790 nm with an energy of 2.4 mJ and a 40 fs full width at half-maximum (fwhm) duration. The laser beam was split into separate pathways for the independent generation of the pump and probe pulses. The pump pulses were produced by a home-built noncollinear optical parametric amplifier (NOPA).[32] For temperature-dependent studies, a single NOPA generated 630 nm light with a 20 nm fwhm bandwidth at 300 nJ/pulse. For the dual-excitation wavelength interleaved pump–probe (DEWI-PP), two NOPAs were used to generate 600 and 650 nm pump pulses at a 20 nm bandwidth and powers of 300 and 200 nJ, respectively. Broadband white-light probe pulses (300–770 nm) were generated by focusing a portion of the fundamental 790 nm pulses into a slowly translating 2 mm CaF$_2$ crystal. These probe pulses were mechanically delayed with respect to the pump pulses by a computer-controlled linear motor stage (Newport IMS 600LM), which provided a maximal delay of 7 ns.

The pump pulses were mechanically chopped at 500 Hz to generate a Pump-ON and Pump-OFF sequence. For DEWI-PP, two choppers mechanically chopped two excitation pulses at frequencies of 500 and 250 Hz to generate four pulse sequences (each 1 ms): Pump-1-ON/Pump-2-OFF/Probe, Pump-1-OFF/Pump-2-ON/Probe, Pump-1-ON/Pump-2-On/Probe, and Pump-1-OFF/Pump-2-OFF/Probe. These pulse sequences allowed nearly simultaneous (separated by milliseconds) pump–probe measurements of two different excitation pulses on the same sample. Thus, the DEWI-PP approach ensures that the primary experimental variable is the excitation energy, which was successfully utilized previously to study excitation-dependent dynamics in carotenoids and phytochrome-related CBCRs.[10]

After being temporally and spatially overlapped with the pump pulses in the Cph1Δ sample, the broadband probe light was detected by an imaging spectrograph (Oriel MS 127) equipped with a 256 pixel photodiode array (Hamamatsu S3901 and C7884). The resulting transient absorption signals had an ∼100 fs temporal resolution [instrumental response function (IRF)], estimated by the rise of the excited-state absorption (ESA) band at 490 nm. The polarizations of pump and probe pulses were set at 54.7° (magic angle) with respect to each other to eliminate any anisotropic effects to the signals.

The pump beam size was significantly greater (3-fold) than the probe beam size at the sample to eliminate any aberrations due to spatial chirp of pump and probe beams, which was confirmed by dithering the pump pulse a little to show the uniform decay of the signals.

The samples were passed continuously through a quartz 2 mm flow cell that was back illuminated with a 720 nm LED light source (Epitex Inc., model L720-66-60). For temperature-dependent studies, a refrigerating circulator (Fisher Scientific Isotemp 1016D) circulated water at 8, 25, and 40 °C to a custom-made bath in contact with a sample bath in the flow system. Before an experiment, the sample was circulated at a set temperature for 10 min to ensure temperature equilibration.

SVD Analysis. The temperature-dependent absorbance spectra of WT were analyzed with MATLAB version 7.11.0. Two SVD vectors were extracted, and the two basis sets, photoactive and fluorescent basis, were constructed by the linear combination of the two vectors with a good fit. Modified Gibbs−Helmholtz equation fitting to a van't Hoff plot based on a SVD analysis concentration was simulated by MATLAB Curve Fitting Toolbox version 3.0.

■ RESULTS

WT Cph1Δ and YH Variant Spectra Exhibit Distinct Temperature Dependence. Fluorescence spectra for WT and YH at 25 °C are both shown in Figure 2. WT and YH have
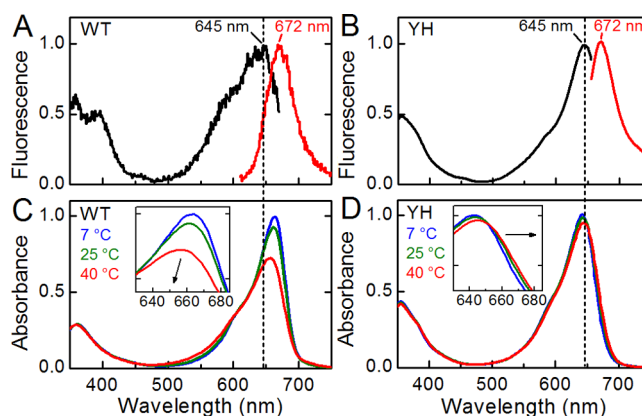

Figure 2. Static measurements on the P$_r$ state of Cph1Δ. Static fluorescence excitation (black) and emission (red) with peak wavelengths indicated in respective color (A and B) and absorption (C and D) spectra are shown for WT (A and C) and YH (B and D) Cph1Δ. Absorption spectra at indicated temperatures are shown; the arrow in the inset emphasizes the spectral shifting of the peak as a function of increasing temperature. The vertical dash indicates 645 nm.

identical maxima at 645 and 672 nm (excitation and emission, respectively). Consistent with previous work,[17,18] the absorption maximum of WT Cph1Δ at 25 °C is significantly red-shifted relative to the excitation maximum (Figure 2C, red curve). The absorption maximum of YH at 25 °C is the same as the fluorescence excitation maximum at 645 nm (Figure 2D, red curve). The absorption spectra for WT and YH were both temperature-dependent; the observed changes were fully reversible in the range from 4 to 43 °C (Figure S1 of the Supporting Information). As previously reported,[17,18] WT exhibits an isosbestic point at 600 nm with the absorption maximum blue shifting with a decrease in temperature (Figure 2C, inset), approaching that of the excitation spectrum. The absorbance also decreases in the peak region (∼660 nm) while

increasing on the blue shoulder at <600 nm. In contrast, YH exhibits a different temperature dependence (Figure 2D): the peak absorbance decreases with an increase in temperature, and the absorption maximum undergoes a slight red shift with an isosbestic point at a much longer wavelength (655 nm). These observations are consistent with the presence of a blue-shifted population in the WT that is increasingly populated at high temperatures, a population that may predominate in the fluorescent, blue-shifted YH variant.

WT Cph1Δ Exhibits Inverted Arrhenius Excited-State Kinetics. Because the temperature dependence of static spectra can be interpreted many ways, we collected pump−probe (PP) transient absorption spectra for both WT and YH at 8, 25, and 40 °C using the same excitation pulse at 630 nm (Figure 3 and
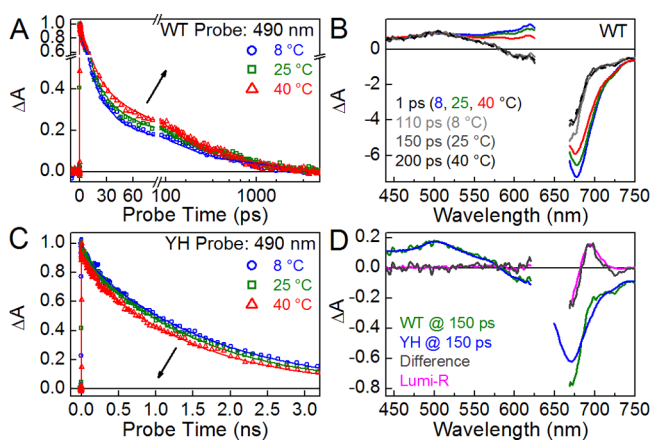

Figure 3. Temperature-dependent PP spectroscopy. PP experiments were performed at 8, 25, and 40 °C (blue, green, and red, respectively). (A and C) Kinetic traces are shown at 490 nm for WT and YH Cph1Δ. Arrows indicate the trend with an increase in temperature. These kinetic traces are fit with respective global analysis models (Figure 5 and Figure S4I−L of the Supporting Information). (B) Comparison of early (at 1 ps) and later (scaled by 5.5-fold, at 110, 150, and 200 ps for 8, 25, and 40 °C, respectively) transient spectra of WT. (D) Comparison between the 25 °C WT and $Y_{176}H$ transient spectra at 150 ps, with a difference between them (gray) compared to Lumi-R (magenta).

Figure S2 of the Supporting Information). PP signals at each temperature were scaled to the initial amplitude of the 490 nm band of excited-state absorption (ESA), where other overlapping signals such as ground-state bleach, stimulated emission, and Lumi-R absorption are minimized or absent (Figure S2 of the Supporting Information). Data in Figure 3 are thus normalized to the initial excited-state P_r* population to allow meaningful comparison of the excited-state signals and Lumi-R quantum yields (Φ_{photo}). YH exhibited an excited-state decay significantly slower than that of WT (Figure 3), consistent with single-molecule studies of this variant.[12,33] YH exhibited standard Arrhenius kinetics, i.e., faster excited-state decay at elevated temperatures. WT instead exhibited inverted Arrhenius kinetics, with slower excited-state decay at elevated temperatures. Inverse temperature effects have previously been described for photoactive proteins. For example, proton dissociation in GFP[34] and the adduct formation reaction in the flavin-based blue light sensors of the LOV (light, oxygen, voltage) family[35] show slower kinetics at elevated temperatures. For these proteins, an apparent transition temperature that separates regimes with positive and negative activation energies

was observed.[36] These observations support conformational transitions that activate or deactivate certain reaction pathways, which imply the existence of a heterogeneous mixture of conformations near the transition temperature.

Excited-State Decay of the YH Variant Matches That of a WT Subpopulation. We employed a two-step procedure to analyze the transient data. First, we decomposed the temperature-dependent PP signals for both proteins using global analysis with a sequential model (Figures S3 and S4 of the Supporting Information).[37,38] In the second step, global analysis using a target model to describe the underlying populations was conducted following further data collection (see below). The sequential model analyzed PP signals by extracting a finite number of exponentially decaying and sequentially interconverting spectral components with fixed difference spectra (evolution-associated difference spectrum or EADS, termed wtEADS and yhEADS for WT and YH, respectively). Good fitting of the WT and YH signals at each temperature required seven and four populations, respectively (wtEADS1−wtEADS7 and yhEASD1−yhEADS4, respectively). At 25 °C, WT exhibited multiexponential dynamics with relaxation times (τ) of 120 fs, 2.3 ps, 13 ps, 99 ps, and 800 ps and a nondecaying population (Figure S3A−C of the Supporting Information). YH Cph1Δ also exhibited multiexponential dynamics, with τ values of 120 fs, 9 ps, 120 ps, and 1.6 ns (Figure S4I−L of the Supporting Information). Comparable, but not identical, lifetimes were observed for the respective proteins at other temperatures (Figures S3 and S4 of the Supporting Information).

At 1 ps, WT Cph1Δ exhibited a greater absolute amplitude from 525 to 700 nm at 8 °C than at 25 and 40 °C signals (Figure 3B), well represented by wtEADS2 (Figure S4B of the Supporting Information). At later times, this difference was lost, well represented by wtEADS4 (Figure 3B and Figure S4C of the Supporting Information). Thus, temperature-dependent effects are more notable at short times and are lost after approximately 100 ps. After 150 ps, the WT and YH signals at 25 °C differed only in the 650−750 nm region (Figure 3D). Notably, the difference between them was identical to that exhibited by the Lumi-R spectrum (Figure 3D), indicating that the only difference between WT and YH signals at 150 ps is Lumi-R formation in WT. A 1−2% photoactivity that is expected for YH[12] could not be resolved in the current data. These results thus demonstrate that the slower phases of excited-state decay in WT are spectrally equivalent to those of the fluorescent, photochemically compromised YH variant, which is further supported by the 8 and 40 °C transient signals (Figure S3 of the Supporting Information).

On the basis of this spectral equivalence, the "crossover region" between 580 and 630 nm can indicate the relative amplitude of a YH-like population in WT. YH shows a consistent negative amplitude in this region, while WT shows a positive amplitude at short times [<50 ps (Figure S2 of the Supporting Information)]; therefore, a negative amplitude correlates with the depletion of a YH-like population. Moreover, a negative amplitude also correlates with temperature. For example, a negative amplitude at 605 nm under the same excitation energy condition is greater at 40 °C than at 25 and 8 °C (Figure S2F of the Supporting Information). These results provide a potential explanation for the inverted Arrhenius effect of WT: a subpopulation with slower excited-state dynamics similar to those of YH becomes increasingly significant at higher temperatures.

WT Cph1Δ Mimics the YH Variant at Short Excitation Wavelengths. A YH-like subpopulation in WT would be preferentially excited at shorter wavelengths, because the YH variant is blue-shifted relative to the WT absorption band and instead matches the WT fluorescence excitation band (see above). We therefore undertook a dual-excitation wavelength interleaved pump−probe (DEWI-PP) study on both proteins (Figure S5 of the Supporting Information). In DEWI-PP,[10] two independent PP experiments are performed simultaneously with a train of alternating excitation pulses differing in center wavelength and/or line shape. This approach minimizes experimental variation such as sample degradation, flow rate, temperature, and laser stability. We used pulses centered at 600 and 670 nm (Figure 4A) to target the putative YH-like and WT populations, respectively.
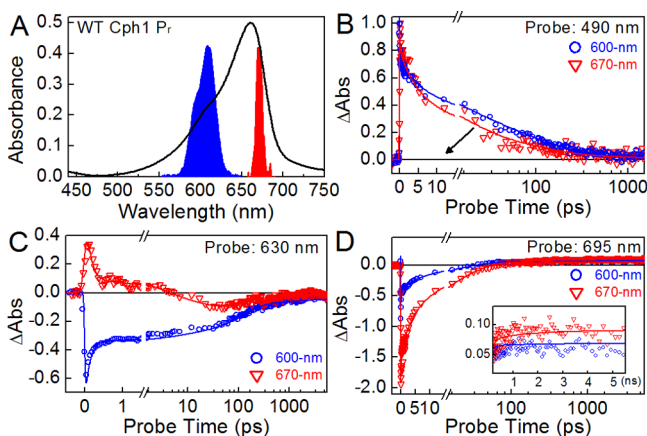

Figure 4. DEWI-PP of WT Cph1Δ. (A) Absorbance of WT P_r overlaid with excitation spectra at 600 and 670 nm (blue and red, respectively). (B and C) Excitation wavelength-dependent kinetic traces at 490 and 630 nm, respectively. (D) Excitation wavelength-dependent quantum yields of Lumi-R represented by a 695 nm probe wavelength. These kinetic traces were fit with a global target model (Figure 5).

WT Cph1Δ exhibited pronounced excitation wavelength dependence in DEWI-PP (Figure S5B,C of the Supporting Information). Decay kinetics of P_r* at 490 nm are distinctly slower after initiation with 600 nm light than with 670 nm light (Figure 4B). At 630 nm, in the crossover region, excitation at 600 nm results in a negative amplitude that persists beyond the experimental time scale (Figure 4C). By contrast, excitation at 670 nm results in an initial positive amplitude that decays to a negative amplitude by 10 ps. At 695 nm, the peak of the Lumi-R absorption band (Figure 3D), excitation wavelength-dependent quantum yield is clearly resolved, with the higher-energy excitation at 600 nm having a Φ_{photo} that is lower than the lower-energy excitation at 670 nm (Figure 4D).

The YH variant also exhibited wavelength-dependent effects in DEWI-PP (Figure S5H,I of the Supporting Information). For example, 670 nm excitation produced a more pronounced negative amplitude in the region assigned to ground-state bleach and stimulated emission. However, the excited-state decay kinetics of YH Cph1Δ exhibited negligible wavelength dependence (Figure S5J of the Supporting Information), demonstrating that the kinetic effects observed with WT Cph1Δ are an authentic property of the protein scaffolding and are not an artifact of the DEWI-PP experiment on the PCB chromophore.

Integrated Analysis of Cph1Δ Dynamics. Our studies demonstrate that WT Cph1Δ exhibits discrepant absorption and fluorescence excitation maxima, temperature effects on absorption spectra, inverted Arrhenius excited-state dynamics, multiphasic excited-state decay, including a component mimicking that of the YH variant, and excitation wavelength-dependent photodynamics. These results are consistent with a heterogeneous P_r ground state in WT Cph1Δ. We therefore used a heterogeneous target model in the second step of data analysis. An integrated model with five subpopulations (Figure 5) was constructed to describe the effects of temperature and
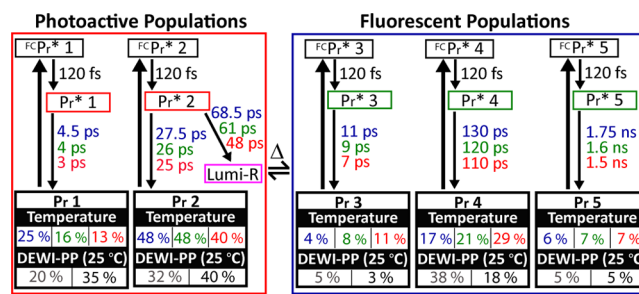

Figure 5. Integrated target model for both PP experiments. P_r 1−5 reflect subpopulations in thermal equilibrium, where P_r 1 and 2 are red-shifted subpopulations and P_r 3−5 are blue-shifted subpopulations. The relative amplitude of initially excited subpopulations under different experimental conditions is indicated. Parameters for 8, 25, and 40 °C are colored blue, green, and red, respectively. DEWI-PP was performed at 25 °C, and occupancy parameters are color-coded as gray and black for 600 and 670 nm excitation, respectively.

excitation wavelength within the framework of global target analysis.[37,38] Target analysis extracts time-independent spectra (species-associated difference spectra) or SADS (Figures S4E−H and S6E−H of the Supporting Information) and corresponding time-dependent concentration profiles for the constituent (sub)populations in the model (Figure S7 of the Supporting Information). Each SADS represents the spectrum of a particular microscopic subpopulation within the postulates of the model and its underlying connectivity scheme. Key features of the target model are presented below, with further details in the Supporting Information.

(1) Five subpopulations coexist in thermal equilibrium, grouped into two spectrally distant categories: the fast-decaying "photoactive" (P_r 1 and 2) and slow-decaying "fluorescent" populations (P_r 3−5). For each subpopulation, the initial 120 fs decay from the sequential model (Figure S3 of the Supporting Information) is assigned as Franck−Condon relaxation. The latter are spectrally and kinetically identical to those of YH Cph1Δ (Figures S4I−L and S6I−L of the Supporting Information for temperature-dependent and DEWI-PP signals, respectively). While P_r 1 and 2 share identical SADS (Figure S4E−H and S6E−H of the Supporting Information) and are thought to have the same static absorption spectrum, only P_r 2 generates Lumi-R. Similar heterogeneity was also observed in phytochrome-related cyanobacteriochrome NpR6012g4 photodynamics.[9]

(2) Each subpopulation exhibits normal Arrhenius kinetics, with a higher temperature inducing faster P_r* decay kinetics. The inverted Arrhenius kinetics observed in WT Cph1Δ (Figure 3A) are explained by temperature-dependent changes in the occupation of P_r subpopulations: for example, at 8 °C, the 630 nm pump-induced occupancies of photoactive and

fluorescent P_r^* populations are 73 and 27%, respectively [P_r 1 + P_r 2 and P_r 3 + P_r 4 + P_r 5, respectively (Table 1)], while they are 64 and 36% at 25 °C and 53 and 47% at 40 °C, respectively (Figure 5 and Table 1).

Table 1. Initial Occupancies of Each Subpopulation under Each Experimental Condition of Temperature and Excitation Pulse Energy[a]

	photoactive population occupancy (%)			fluorescent population occupancy (%)			
	P_r 1	P_r 2	total	P_r 3	P_r 4	P_r 5	total
temperature dependence (630 nm excitation)							
8 °C	25	48	73	4	17	6	27
25 °C	16	48	64	8	21	7	36
40 °C	13	40	53	11	29	7	47
excitation energy dependence (at 25 °C)							
600 nm excitation	20	32	52	5	38	5	48
670 nm excitation	35	40	75	3	18	5	26

[a]The five subpopulations, P_r 1−5, are categorized as photoactive (P_r 1 and 2) and fluorescent (P_r 3−5) populations. These parameters are based on the target model from Figure 5.

(3) Excitation wavelength dependence is modeled on the basis of the kinetic parameters obtained at 25 °C with the 630 nm pump pulse by varying only the initial occupancy of P_r^*. For 600 nm excitation, the photoactive/fluorescent P_r^* population ratio is modeled as 52/48, while for 670 nm excitation, the ratio is 75/25 (Table 1).

(4) The model predicts Φ_{photo} values of 9.5 and 12% for the 600 and 670 nm excitation signals, respectively (Figure S7D of the Supporting Information and Table 2). For 630 nm

Table 2. Lumi-R Quantum Yields (Φ_{Lumi-R}) under Each Experimental Condition of Temperature and Excitation Pulse Energy[a]

	P_r 2 occupancy (%)	branching % to Lumi-R	Φ_{Lumi-R} (%)
temperature dependence (630 nm excitation)			
8 °C	48	29	14
25 °C	48	30	14.4
40 °C	40	34	13.6
excitation energy dependence (at 25 °C)			
600 nm excitation	32	30	9.6
670 nm excitation	40	30	12

[a]The branching ratio is calculated based on τ (P_r 2* → P_r 2) and τ (P_r 2* → Lumi-R) in Figure 5. The Φ_{Lumi-R} is calculated by P_r 2 occupancy × branching % to Lumi-R.

excitation, Φ_{photo} was temperature-independent at approximately 14% (Figure S7A−C of the Supporting Information and Table 2). With 630 nm excitation, apparent temperature independence arises due to offsetting factors: the photoactive P_r 2 population is excited less efficiently at 40 °C, but the efficiency of Lumi-R generation is higher. Lower-energy excitation (670 nm) selectively excites more of P_r 2 (Figure 5).

(5) SADS are temperature-independent (Figure S4E−H of the Supporting Information). DEWI-PP SADS of WT Cph1Δ

are excitation wavelength-dependent (Figure S6E−H of the Supporting Information), likely because of an intrinsic red-edge effect.[39] SADS of "fluorescent populations" from DEWI-PP signals (Figure S6G of the Supporting Information) qualitatively reproduce DEWI-PP signals from YH Cph1Δ (Figure S6I−L of the Supporting Information).

The resulting model provides a good fit to both temperature-dependent PP signals and DEWI-PP signals (Figures S2 and S5 of the Supporting Information). For example, the wtEADS6 derived from sequential analysis (corresponding to Lumi-R formation) showed a slight discrepancy in the Lumi-R peak wavelength for the two DEWI-PP data sets (Figure S6D of the Supporting Information). Such a discrepancy is not seen for the Lumi-R SADS from the target model (Figure S6H of the Supporting Information). Moreover, the target model correctly predicts the inverse Arrhenius effect (Figure 3), excitation wavelength-dependent kinetics (Figure 4), and excitation wavelength-dependent quantum yield (Figure 4).

Modeling the Inverted Arrhenius Effect. The excellent agreement of the model in fitting both the temperature-dependent and DEWI-PP signals (Figure 5) strongly supports the underlying dynamic heterogeneity hypothesis. As a model describing the behavior of the excited-state populations, it formally describes the distribution of excited-state subpopulations generated by a given excitation. We therefore sought similar information about the P_r ground state. We applied singular-vector decomposition (SVD) (Figure 6) of the temperature-dependent absorption spectra (Figure S1D−F of
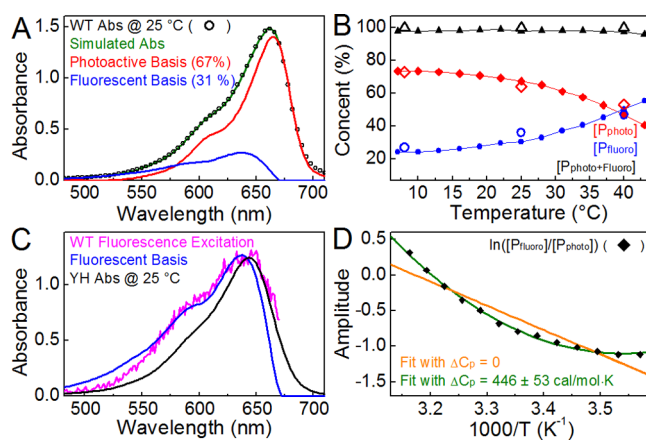

Figure 6. SVD analysis of temperature-dependent absorbance spectra of WT. (A) Photoactive (red) and fluorescent (blue) bases representing P_r 1 and 2 and P_r 3−5, respectively, are compared to the WT absorbance spectra (black) at 25 °C. WT was simulated (green) as 67% photoactive and 31% fluorescent. (B) Temperature-dependent concentrations of photoactive and fluorescent bases were determined for static measurements using SVD (red diamonds and blue circles, respectively) and are compared to those estimated by temperature-dependent PP (empty diamonds and circles). (C) The fluorescent basis (blue) is compared to the YH absorption spectrum at 25 °C (black) and the WT fluorescence excitation spectrum (magenta). (D) van't Hoff plot for WT Cph1Δ subpopulations extracted from SVD concentrations from panel B. Data were fit to a standard model (orange, $\Delta C_p = 0$) and eq 1 (green). The thermodynamic parameters with a standard model fit are as follows (at 25 °C): $\Delta S = 21.4 \pm 2.3$ cal mol^{-1} K^{-1}, $\Delta H = 6.76 \pm 0.68$ kcal/mol, and $\Delta G = 364$ cal/mol. Parameters with a fitting according to eq 1: $\Delta C_p = 446 \pm 53$ cal mol^{-1} K^{-1}, $\Delta S = 22.1 \pm 0.9$ cal mol^{-1} K^{-1}, $\Delta H = 7.05 \pm 0.27$ kcal/mol, and $\Delta G = 458$ cal/mol.

the Supporting Information) to estimate the absolute ratio of ground-state subpopulations. In analyzing the transient signals, we had postulated that the subpopulations within the fluorescent and photoactive categories were spectrally indistinguishable. We therefore used only two bases, fluorescent and photoactive, in analyzing the static spectra. The calculated fluorescent basis is blue-shifted relative to that of WT (Figure 6A) and is similar to that of YH (Figure 6C), overlapping well with the WT fluorescence excitation spectrum (Figure 6C). The photoactive basis is red-shifted relative to the fluorescent basis, as expected. The temperature-dependent ground-state subpopulation partitioning obtained from SVD is also consistent with the partitioning estimated from the integrated model for the temperature-dependent signals (Figure 6B). This analysis thus quantitatively reproduces the static spectral behavior of WT Cph1Δ and is consistent with the heterogeneous target model. Moreover, the equivalent distributions obtained for static and transient signals indicate that the heterogeneity arises in the P_r ground state and that the distribution of ground-state subpopulations gives rise to an equivalent distribution of excited-state subpopulations.

SVD analysis also allowed us to examine the subpopulation partitioning in the static spectra in more detail, which gave the ratio of photoactive and fluorescent populations at each temperature, allowing derivation of the equilibrium constant for their interconversion at that temperature. This allows construction of a van't Hoff plot (Figure 6D), which demonstrates a nonlinear relationship of ln K versus $1/T$. Such nonlinear van't Hoff plots are often observed in protein folding studies and are indicative of a change in heat capacity (ΔC_p) between folded and unfolded states. A similar interpretation can readily be applied to photoactive and fluorescent subpopulations if one assumes that they are structurally different. Assuming that ΔC_p is constant in the temperature range being studied here and is defined as $C_p(\text{fluorescent}) - C_p(\text{photoactive})$, the change in the free energy for photoactive–fluorescent interconversion would follow eq 1:

$$\Delta G(T) = \Delta H_m\left(1 - \frac{T}{T_m}\right) + \Delta C_p\left[(T - T_m) - T \times \ln\left(\frac{T}{T_m}\right)\right] \tag{1}$$

where T_m is a reference temperature (25 °C) and ΔH_m is the change in enthalpy at that temperature.[40,41] Employing the standard relationship between free energy change ΔG and equilibrium constant K allows the van't Hoff plot to be fit with eq 1 (Figure 6D, green curve), resulting in good agreement with the observed data with a ΔC_p of 446 cal mol^{-1} K^{-1}. Agreement is much poorer if the data are instead fit to a standard linear relationship with a ΔC_p of 0 (Figure 6D, orange curve). This analysis demonstrates that the static spectra are described well by the target model and that there is a change in heat capacity upon fluorescent–photoactive interconversion.

We also analyzed the Arrhenius kinetics of the microscopic rate constants derived from target analysis of temperature-dependent PP studies (Figure 5). The fast relaxation process with 120 fs is temperature-independent, consistent with Franck–Condon relaxation after photoexcitation. Evolution of the relaxed excited-state subpopulations follows normal Arrhenius kinetics. Surprisingly, the activation energies (E_a) show an unexpected pattern: the fast-decaying P_r 1 and 3 subpopulations have E_a values (2.2−2.5 kcal/mol) greater than

those of slow-decaying subpopulations P_r 2, 4, and 5 (∼0.9 kcal/mol) (Figure S1G,H of the Supporting Information). There is thus an inverse correlation between relaxation time and activation energy in WT Cph1Δ, despite the direct correlation between relaxation time and temperature arising from standard Arrhenius behavior. This indicates that the observed rate constants for excited-state decay in WT Cph1Δ are largely determined by the Arrhenius pre-exponential coefficient, A, instead of E_a. These data thus confirm standard Arrhenius behavior of the microscopic subpopulations while also demonstrating that there is not a simple correlation between excited-state decay and excited-state activation energy.

■ DISCUSSION

In this report, we have characterized the forward reaction of the model cyanobacterial phytochrome Cph1Δ providing new insight into the temperature- and excitation wavelength-dependent static and ultrafast photodynamic properties. These studies provide compelling support for a heterogeneous P_r ground state in Cph1Δ, in which a blue-shifted, fluorescent population is in equilibrium with a photoactive population peaking at longer wavelengths. Our results therefore corroborate solid-state NMR[30] and fluorescence[18,19] measurements, although such previous studies were performed on samples held at much lower temperatures. We also show that interconversion between these two forms of Cph1Δ is accompanied by a change in heat capacity, indicative of a structural rearrangement with a change in buried nonpolar surface area.[40,41] The ΔC_p for WT Cph1Δ is significantly lower than that observed for protein unfolding[41] and that observed for the pB-to-pG transition in photoactive yellow protein (PYP), which is known to involve a partial loss of structure.[42] The rearrangement of Cph1Δ thus seems likely to involve a large-scale conformational change rather than denaturation or loss of secondary structure. Such structural heterogeneity is a challenging issue for crystallographic analysis because of the constraints associated with crystallization, and the potential for selection of a conformation(s) that preferentially crystallizes.[30]

It presently is unclear whether other phytochromes show similar behavior. Temperature dependence has been reported in static measurements; in both oat phytochrome A[43,44] and the bacteriophytochrome Agp1,[45] effects that are somewhat similar to those reported for Cph1Δ. The temperature dependence of the ultrafast photodynamics of plant phytochromes has not yet been analyzed. However, previous studies of the excitation wavelength dependence in Cph1Δ have produced conflicting interpretations: an initial PP study with single-wavelength detection produced results similar to ours, with slower dynamics at shorter wavelengths.[22] A more recent study by van Thor and coworkers with broadband detection resolved sequential EADS with the same spectra trends we report in the crossover region, although these data were interpreted differently since they were unable to resolve the kinetic differences the DEWI-PP approach extracts.[23] The P_r state of phytochromes has also been examined using vibrational methods. In particular, a femtosecond resonance Raman study of Cph1Δ was interpreted in terms of complete photoisomerization on the excited-state surface due to rapid formation of Lumi-R bands with a time constant faster than that of excited-state decay.[15] Such an interpretation requires a homogeneous population, so our results call this conclusion into question.[31] Similarly, Raman intensity analysis was used to model the absorption band of Cph1Δ in solution or in crystals

as a single homogeneous population.[17] This analysis used values of the homogeneous broadening constant, Γ, significantly higher than those that have been reported for other proteins, and hole-burning experiments were not conducted to provide independent support for this Γ value. We have performed two independent ultrafast measurements, and the successful fitting of both ultrafast inverse Arrhenius effects and static temperature effects provides powerful additional evidence of our target model.

In addition to its implications for the interpretation of spectroscopic studies, our work provides new insight into the means by which phytochromes partition the excited-state population between fluorescence and photochemistry. The red-shifted subpopulations must have a chromophore configuration and/or protein−chromophore interactions slightly different from those of the blue-shifted subpopulations. Moreover, the difference in heat capacity between the two categories implies the existence of two distinct configurations of the protein. Mutations such as $Y_{176}H$ would thus seem to change the equilibrium between these configurations. Such configurational heterogeneity has physiological implications, as well. Indeed, the YH mutation in plant phytochromes from *Arabidopsis* has been shown to confer light-independent constitutive signaling phenotypes consistent with a signaling-active protein conformation[46] and the ability to bind to phytochrome-interacting transcription factors in the absence of light.[47] Further engineering of phytochrome will ultimately benefit from elucidation of the protein−chromophore interactions that determine partitioning between potentially signaling-active and -inactive subpopulations.

■ ASSOCIATED CONTENT

Ⓢ Supporting Information

Details of global analysis target model construction, SVD analysis fit over the full temperature range and Arrhenius analysis based on the target model, temperature- and excitation-dependent transient absorption data and their species-associated spectra, with the target model concentration profile. This material is available free of charge via the Internet at http://pubs.acs.org.

■ AUTHOR INFORMATION

Corresponding Author

*Department of Chemistry, University of California at Davis, Davis, CA 95616. E-mail: dlarsen@ucdavis.edu. Telephone: (530) 754-9075.

Notes

The authors declare no competing financial interest.

■ ACKNOWLEDGMENTS

■ ABBREVIATIONS

Cph1Δ, PAS-GAF-PHY photosensory core module of Cph1; WT, wild type; YH, $Y_{176}H$ mutant; CBD, chitin-binding domain; CD, circular dichroism; EADS, evolution-associated difference spectrum; SADS, species-associated difference spectra; DEWI-PP, dual-excitation wavelength interleaved pump−probe; ESI, excited-state intermediate; ESA, excited-state absorption; SE, stimulated emission; GAF, domain name derived from cGMP phosphodiesterase/adenylyl cyclase/FhlA; GSA, ground-state absorbance; RcaE, regulator of chromatic adaptation E; NOPA, noncollinear optical parametric amplifier; PAS, Per-ARNT-Sim; PCB, phycocyanobilin; P_r, red-absorbing ground state of red/far-red phytochromes; P_{fr}, far-red-absorbing photoproduct state of red/far-red phytochromes; Φ, total photocycle quantum yield; Φ_{Lumi}, quantum yield of generating Lumi-R_f; PYP, photoactive yellow protein.

■ REFERENCES

(1) Rockwell, N. C., Su, Y. S., and Lagarias, J. C. (2006) Phytochrome Structure and Signaling Mechanisms. *Annu. Rev. Plant Biol. 57*, 837−858.

(2) Auldridge, M. E., and Forest, K. T. (2011) Bacterial Phytochromes: More Than Meets the Light. *Crit. Rev. Biochem. Mol. Biol. 46*, 67−88.

(3) Franklin, K. A., and Quail, P. H. (2010) Phytochrome Functions in *Arabidopsis* Development. *J. Exp. Bot. 61*, 11−24.

(4) Piatkevich, K. D., Subach, F. V., and Verkhusha, V. V. (2013) Engineering of Bacterial Phytochromes for Near-Infrared Imaging, Sensing, and Light-Control in Mammals. *Chem. Soc. Rev. 42*, 3441−3452.

(5) Shu, X. K., Royant, A., Lin, M. Z., Aguilera, T. A., Lev-Ram, V., Steinbach, P. A., and Tsien, R. Y. (2009) Mammalian Expression of Infrared Fluorescent Proteins Engineered from a Bacterial Phytochrome. *Science 324*, 804−807.

(6) Auldridge, M. E., Satyshur, K. A., Anstrom, D. M., and Forest, K. T. (2012) Structure-guided Engineering Enhances a Phytochrome-based Infrared Fluorescent Protein. *J. Biol. Chem. 287*, 7000−7009.

(7) Sineshchekov, V. A., Frances, S., and White, M. J. (1995) Fluorescence and Photochemical Characterization of Phytochrome in De-Etiolated Pea Mutant Lip. *J. Photochem. Photobiol., B 28*, 47−51.

(8) Anders, K., von Stetten, D., Mailliet, J., Kiontke, S., Sineshchekov, V. A., Hildebrandt, P., Hughes, J., and Essen, L. O. (2011) Spectroscopic and Photochemical Characterization of the Red-Light Sensitive Photosensory Module of Cph2 from *Synechocystis* PCC 6803. *Photochem. Photobiol. 87*, 160−173.

(9) Kim, P. W., Freer, L. H., Rockwell, N. C., Martin, S. S., Lagarias, J. C., and Larsen, D. S. (2012) Femtosecond Photodynamics of the Red/Green Cyanobacteriochrome NpR6012g4 from *Nostoc punctiforme*. 1. Forward Dynamics. *Biochemistry 51*, 608−618.

(10) Kim, P. W., Freer, L. H., Rockwell, N. C., Martin, S. S., Lagarias, J. C., and Larsen, D. S. (2012) Femtosecond Photodynamics of the Red/Green Cyanobacteriochrome NpR6012g4 from *Nostoc punctiforme*. 2. Reverse Dynamics. *Biochemistry 51*, 619−630.

(11) Kim, P. W., Freer, L. H., Rockwell, N. C., Martin, S. S., Lagarias, J. C., and Larsen, D. S. (2012) Second-Chance Forward Isomerization Dynamics of the Red/Green Cyanobacteriochrome NpR6012g4 from *Nostoc punctiforme*. *J. Am. Chem. Soc. 134*, 130−133.

(12) Fischer, A. J., and Lagarias, J. C. (2004) Harnessing Phytochrome's Glowing Potential. *Proc. Natl. Acad. Sci. U.S.A. 101*, 17334−17339.

(13) Glazer, A. N. (1999) Phycobiliproteins. In *Chemicals from Microalgae* (Cohen, A., Ed.) pp 261−280, Taylor & Francis Inc., London.

(14) Holzwarth, A. R., Venuti, E., Braslavsky, S. E., and Schaffner, K. (1992) The Phototransformation Process in Phytochrome. 1. Ultrafast Fluorescence Component and Kinetic-Models for the Initial Pr → Pfr

Transformation Steps in Native Phytochrome. *Biochim. Biophys. Acta 1140*, 59−68.

(15) Dasgupta, J., Frontiera, R. R., Taylor, K. C., Lagarias, J. C., and Mathies, R. A. (2009) Ultrafast Excited-State Isomerization in Phytochrome Revealed by Femtosecond Stimulated Raman Spectroscopy. *Proc. Natl. Acad. Sci. U.S.A. 106*, 1784−1789.

(16) Toh, K. C., Stojkovic, E. A., van Stokkum, I. H. M., Moffat, K., and Kennis, J. T. M. (2010) Proton-Transfer and Hydrogen-Bond Interactions Determine Fluorescence Quantum Yield and Photochemical Efficiency of Bacteriophytochrome. *Proc. Natl. Acad. Sci. U.S.A. 107*, 9170−9175.

(17) Spillane, K. M., Dasgupta, J., Lagarias, J. C., and Mathies, R. A. (2009) Homogeneity of Phytochrome Cph1Δ Vibronic Absorption Revealed by Resonance Raman Intensity Analysis. *J. Am. Chem. Soc. 131*, 13946−13948.

(18) Mailliet, J., Psakis, G., Feilke, K., Sineshchekov, V., Essen, L.-O., and Hughes, J. (2011) Spectroscopy and a High-Resolution Crystal Structure of Tyr263 Mutants of Cyanobacterial Phytochrome Cph1Δ. *J. Mol. Biol. 413*, 115−127.

(19) Sineshchekov, V., Koppel, L., Esteban, B., Hughes, J., and Lamparter, T. (2002) Fluorescence Investigation of the Recombinant Cyanobacterial Phytochrome (Cph1Δ) and Its C-terminally Truncated Monomeric Species (Cph1Δ2): Implication for Holoprotein Assembly, Chromophore-Apoprotein Interaction and Photochemistry. *J. Photochem. Photobiol., B 67*, 39−50.

(20) Essen, L. O., Mailliet, J., and Hughes, J. (2008) The Structure of a Complete Phytochrome Sensory Module in the Pr Ground State. *Proc. Natl. Acad. Sci. U.S.A. 105*, 14709−14714.

(21) Lamparter, T., Mittmann, F., Gartner, W., Borner, T., Hartmann, E., and Hughes, J. (1997) Characterization of Recombinant Phytochrome from the Cyanobacterium *Synechocystis. Proc. Natl. Acad. Sci. U.S.A. 94*, 11792−11797.

(22) Heyne, K., Herbst, J., Stehlik, D., Esteban, B., Lamparter, T., Hughes, J., and Diller, R. (2002) Ultrafast Dynamics of Phytochrome from the Cyanobacterium *Synechocystis*, Reconstituted with Phycocyanobilin and Phycoerythrobilin. *Biophys. J. 82*, 1004−1016.

(23) Fitzpatrick, A. E., Lincoln, C. N., van Wilderen, L. J., and van Thor, J. J. (2012) Pump-Dump-Probe and Pump-Repump-Probe Ultrafast Spectroscopy Resolves Cross Section of an Early Ground State Intermediate and Stimulated Emission in the Photoreactions of the Pr Ground State of the Cyanobacterial Phytochrome Cph1Δ. *J. Phys. Chem. B 116*, 1077−1088.

(24) van Wilderen, L., Clark, I. P., Towrie, M., and van Thor, J. J. (2009) Mid-Infrared Picosecond Pump-Dump-Probe and Pump-Repump-Probe Experiments to Resolve a Ground-State Intermediate in Cyanobacterial Phytochrome Cph1Δ. *J. Phys. Chem. B 113*, 16354−16364.

(25) van Thor, J. J., Ronayne, K. L., and Towrie, M. (2007) Formation of the Early Photoproduct Lumi-R of Cyanobacterial Phytochrome Cph1Δ Observed by Ultrafast Mid-Infrared Spectroscopy. *J. Am. Chem. Soc. 129*, 126−132.

(26) Yang, Y., Linke, M., von Haimberger, T., Hahn, J., Matute, R., Gonzalez, L., Schmieder, P., and Heyne, K. (2012) Real-Time Tracking of Phytochrome's Orientational Changes During Pr Photoisomerization. *J. Am. Chem. Soc. 134*, 1408−1411.

(27) van Thor, J. J., Borucki, B., Crielaard, W., Otto, H., Lamparter, T., Hughes, J., Hellingwerf, K. J., and Heyn, M. P. (2001) Light-Induced Proton Release and Proton Uptake Reactions in the Cyanobacterial Phytochrome Cph1Δ. *Biochemistry 40*, 11460−11471.

(28) Rohmer, T., Lang, C., Bongards, C., Gupta, K., Neugebauer, J., Hughes, J., Gartner, W., and Matysik, J. (2010) Phytochrome as Molecular Machine: Revealing Chromophore Action during the Pfr → Pr Photoconversion by Magic-Angle Spinning NMR Spectroscopy. *J. Am. Chem. Soc. 132*, 4431−4437.

(29) Mroginski, M. A., von Stetten, D., Escobar, F. V., Strauss, H. M., Kaminski, S., Scheerer, P., Gunther, M., Murgida, D. H., Schmieder, P., Bongards, C., Gartner, W., Mailliet, J., Hughes, J., Essen, L. O., and Hildebrandt, P. (2009) Chromophore Structure of Cyanobacterial Phytochrome Cph1Δ in the Pr State: Reconciling Structural and

Spectroscopic Data by QM/MM Calculations. *Biophys. J. 96*, 4153−4163.

(30) Song, C., Psakis, G., Lang, C., Mailliet, J., Gartner, W., Hughes, J., and Matysik, J. (2011) Two Ground State Isoforms and a Chromophore D-Ring Photoflip Triggering Extensive Intramolecular Changes in a Canonical Phytochrome. *Proc. Natl. Acad. Sci. U.S.A. 108*, 3842−3847.

(31) Chang, C.-W., Gottlieb, S. M., Kim, P. W., Rockwell, N. C., Lagarias, J. C. L., and Larsen, D. S. (2013) Reactive Ground-State Pathways Are Not Ubiquitous in Red/Green Cyanobacteriochromes. *J. Phys. Chem. B 117*, 11229−11238.

(32) Wilhelm, T., Piel, J., and Riedle, E. (1997) Sub-20-fs Pulses Tunable Across the Visible from a Blue-Pumped Single-Pass Noncollinear Parametric Converter. *Opt. Lett. 22*, 1494−1496.

(33) Miller, A. E., Fischer, A. J., Laurence, T., Hollars, C. W., Saykally, R. J., Lagarias, J. C., and Huser, T. (2006) Single-Molecule Dynamics of Phytochrome-Bound Fluorophores Probed by Fluorescence Correlation Spectroscopy. *Proc. Natl. Acad. Sci. U.S.A. 103*, 11136−11141.

(34) Agmon, N. (2007) Kinetics of Switchable Proton Escape from a Proton-Wire within Green Fluorescence Protein. *J. Phys. Chem. B 111*, 7870−7878.

(35) Nozaki, D., Iwata, T., Tokutomi, S., and Kandori, H. (2005) Unique Temperature Dependence in the Adduct Formation Between FMN and Cysteine S-H Group in the LOV2 Domain of Adiantum Phytochrome3. *Chem. Phys. Lett. 410*, 59−63.

(36) Zaccai, G. (2000) Biochemistry: How Soft is a Protein? A Protein Dynamics Force Constant Measured by Neutron Scattering. *Science 288*, 1604−1607.

(37) Holzwarth, A. R. (1996) Data Analysis of Time-Resolved Measurements. In *Biophysical Techniques in Photosynthesis* (Amesz, J., and Hoff, A. J., Eds.) pp 75−92, Springer, Dordrecht, The Netherlands.

(38) van Stokkum, I. H. M., Larsen, D. S., and van Grondelle, R. (2004) Global and Target Analysis of Time-Resolved Spectra. *Biochim. Biophys. Acta 1657*, 82−104.

(39) Demchenko, A. P. (2002) The Red-Edge Effects: 30 Years of Exploration. *Luminescence 17*, 19−42.

(40) Prabhu, N. V., and Sharp, K. A. (2005) Heat Capacity in Proteins. *Annu. Rev. Phys. Chem.*, 521−548.

(41) Robertson, A. D., and Murphy, K. P. (1997) Protein Structure and the Energetics of Protein Stability. *Chem. Rev. 97*, 1251−1267.

(42) VanBrederode, M. E., Hoff, W. D., VanStokkum, I. H. M., Groot, M. L., and Hellingwerf, K. J. (1996) Protein Folding Thermodynamics Applied to the Photocycle of the Photoactive Yellow Protein. *Biophys. J. 71*, 365−380.

(43) Schmidt, P., Gensch, T., Remberg, A., Gartner, W., Braslavsky, S. E., and Schaffner, K. (1998) The Complexity of the Pr to Pfr Phototransformation Kinetics is an Intrinsic Property of Native Phytochrome. *Photochem. Photobiol. 68*, 754−761.

(44) Sineshchekov, V. A. (2004) Phytochrome A: Functional Diversity and Polymorphism. *Photochem. Photobiol. Sci. 3*, 596−607.

(45) Njimona, I., and Lamparter, T. (2011) Temperature Effects on *Agrobacterium* Phytochrome Agp1. *PLoS One 6*, e25977.

(46) Su, Y.-S., and Lagarias, J. C. (2007) Light-Independent Phytochrome Signaling Mediated by Dominant GAF Domain Tyrosine Mutants of *Arabidopsis* Phytochromes in Transgenic Plants. *Plant Cell 19*, 2124−2139.

(47) Galvao, R. M., Li, M., Kothadia, S. M., Haskel, J. D., Decker, P. V., Van Buskirk, E. K., and Chen, M. (2012) Photoactivated Phytochromes Interact with HEMERA and Promote Its Accumulation to Establish Photomorphogenesis in *Arabidopsis. Genes Dev. 26*, 1851−1863.